PLOS ONE

Sildenafil-evoked photoreceptor oxidative stress *in vivo* is unrelated to impaired visual performance in mice

Bruce A. Berkowitz[1]*, **Robert H. Podolsky**[2], **Karen Lins Childers**[2], **Aicha Saadane**[3], **Timothy S. Kern**[3,4], **Robin Roberts**[1], **Hailey Olds**[1☉], **Joydip Joy**[1☉], **Collin Richards**[1☉], **Tilman Rosales**[1], **Michael Schneider**[1], **Brennan Schilling**[1‡], **Arthur Orchanian**[1‡], **Emma Graffice**[1], **Kenan Sinan**[1], **Haohua Qian**[5], **Lamis Harp**[1]

1 Department of Ophthalmology, Visual and Anatomical Sciences, Wayne State University School of Medicine, Detroit, Michigan, United States of America, 2 Beaumont Research Institute, Beaumont Health, Royal Oak, Michigan, United States of America, 3 Gavin Herbert Eye Institute, University of California Irvine, Irvine, California, United States of America, 4 Veterans Administration Medical Center Research Service, Long Beach, California, United States of America, 5 Visual Function Core National Eye Institute, National Institutes of Health, Bethesda, Maryland, United States of America

☉ These authors contributed equally to this work.
‡ These authors also contributed equally to this work.
* baberko@med.wayne.edu

Abstract

Purpose

The phosphodiesterase inhibitor sildenafil is a promising treatment for neurodegenerative disease, but it can cause oxidative stress in photoreceptors *ex vivo* and degrade visual performance in humans. Here, we test the hypotheses that in wildtype mice sildenafil causes i) wide-spread photoreceptor oxidative stress *in vivo* that is linked with ii) impaired vision.

Methods

In dark or light-adapted C57BL/6 mice ± sildenafil treatment, the presence of oxidative stress was evaluated in retina laminae *in vivo* by QUEnch-assiSTed (QUEST) magnetic resonance imaging, in the subretinal space *in vivo* by QUEST optical coherence tomography, and in freshly excised retina by a dichlorofluorescein assay. Visual performance indices were also evaluated by QUEST optokinetic tracking.

Results

In light-adapted mice, 1 hr post-sildenafil administration, oxidative stress was most evident in the superior peripheral outer retina on both *in vivo* and *ex vivo* examinations; little evidence was noted for central retina oxidative stress *in vivo* and *ex vivo*. In dark-adapted mice 1 hr after sildenafil, no evidence for outer retina oxidative stress was found *in vivo*. Evidence for sildenafil-induced central retina rod cGMP accumulation was suggested as a panretinally thinner, dark-like subretinal space thickness in light-adapted mice at 1 hr but not 5 hr post-sildenafil. Cone-based visual performance was impaired by 5 hr post-sildenafil and not corrected with anti-oxidants; vision was normal at 1 hr and 24 hr post-sildenafil.

Conclusions

The sildenafil-induced spatiotemporal pattern of oxidative stress in photoreceptors domi-
nated by rods was unrelated to impairment of cone-based visual performance in wildtype
mice.

Introduction

Sildenafil, an inhibitor of phosphodiesterase type 5 (PDE 5, the enzyme responsible for cGMP
hydrolysis), is useful for the treatment of erectile dysfunction and pulmonary arterial hyper-
tension, and has been suggested as a potential therapeutic in neurodegenerative diseases
including age-related macular degeneration and Alzheimer's disease [1–4]. However, benefits
from sildenafil therapy may be limited by its visual side effects that can range from mild to
severe. For example, sildenafil can temporarily affect visual performance (although more per-
sistent responses have been reported), and most electrophysiology studies in healthy retina
have demonstrated a short-term negative impact [3, 5–10]. Of greater concern, sildenafil usage
has been linked to idiopathic serous macular detachment [11]. In addition, sildenafil may
increase the risk of neurodegeneration in, for example, the 1 in 50 people who are potential
carriers of sight-threatening genetic defects underlying retinitis pigmentosa [12, 13]. Thus, a
better understanding of the consequences of sildenafil on the visual system is needed to miti-
gate its side effects.

The above side effects in retina are commonly thought to arise from inhibition of PDE 5
located in cells of the inner retina and in the retinal pigment epithelium, as well as from inhibi-
tion of PDE 6 found in photoreceptors [14, 15]. One hypothesized consequence of such inhibi-
tion is a greater-than-normal cGMP content causing cyclic nucleotide-gated channels to
remain open even in the light, resulting in widespread oxidative stress via increased intracellu-
lar calcium levels and ion pumping [16–19]. In photoreceptor cells *ex vivo*, phosphodiesterase
inhibition causes excessive production of free radicals (i.e., oxidative stress), but it is unclear if
this happens *in vivo* [17, 18]. Photoreceptor oxidative stress *per se* can impair visual perfor-
mance by an unclear mechanism that may include acidification of the subretinal space [20–
27].

In this study, we tested if sildenafil evokes panretinal oxidative stress in healthy retina *in
vivo* and whether an induced oxidative stress is linked with impaired visual performance. Oxi-
dative stress is non-invasively evaluated in retinal laminae using QUEnch-assiSTed (QUEST)
magnetic resonance imaging (MRI), in subretinal space using QUEST optical coherence
tomography (OCT), and in cone-based vision with QUEST optokinetic tracking (OKT) [20,
24, 28, 29]. QUEST MRI accurately evaluates panretinal, layer-specific, paramagnetic free radi-
cal-generated contrast as a decrease in 1/T1 with anti-oxidants [29, 30]. QUEST MRI oxidative
stress measurements have been validated in animal models against several *ex vivo* assays [29].
In addition, we have shown positive QUEST MRI controls for localized oxidative stress only in
certain parts of the retina, including treatment with either sodium iodate or diltiazem, or
mutant mice with cre-dependent retinal pigment epithelium (RPE)-specific MnSOD knockout
mice or PDE6b damage (rd10 mice) [20, 28, 31–33]. QUEST OCT tests whether anti-oxidants
increase the light-adapted external limiting membrane to retinal pigment epithelium
(ELM-RPE) thickness in central retina which is suppressed by oxidative stress, perhaps via
induced acidosis [24–27]. The *in vivo* results were compared to conventional dichlorofluores-
cein (DCF) fluorescent maps of steady-state levels of reactive oxygen species in freshly excised
retina [34]. Finally, QUEST OKT was used as a validated test of whether oxidative stress

impaired cone-based visual performance [20]. Control mice were evaluated in groups given either sildenafil + saline, or sildenafil + an anti-oxidant drug combination that reduces excessive production of reactive oxygen species [i.e., methylene blue (MB) and α-lipoic acid (ALA)]. MB is an alternate electron transporter that effectively suppresses generation of superoxide from a variety of sources; ALA is a potent free radical neutralizer; both are FDA approved and are useful for QUEST MRI, OCT, and OKT studies [20, 24, 29, 35, 36].

Materials and methods

All mice were treated in accordance with the National Institutes of Health Guide for the Care and Use of Laboratory Animals, the Association for Research in Vision and Ophthalmology Statement for the Use of Animals in Ophthalmic and Vision Research, and with specific authorization by the Wayne State University Division of Laboratory Animal Resources (DLAR) Institutional Animal and Care Use Committee (IACUC), and by National Eye Institute Animal Care and Use Committee. 2 mo male C57BL/6J mice (Jackson Laboratories, ME) were housed and maintained in full dark conditions or 12 hr:12 hr light-dark cycle laboratory lighting. Mice were humanely euthanized by an overdose of urethane followed by a cervical dislocation, as detailed in our IACUC-approved protocol. Data were collected from the left eye except for the OKT examination which used both eye's.

QUEST MRI

QUEST MRI was performed as previously described [20, 28, 29, 32, 33]. Mice were maintained in darkness for at least 16 hrs before all MRI studies. High-resolution MRI data were acquired on a 7T system (Bruker ClinScan, Billerica, MA) using a receive-only surface coil (1.0 cm diameter) centered on the left eye. One group of mice were kept in the dark ("dark") throughout the preparation and MRI examination. For the light study, another group of mice ("light") were exposed to room light (~ 300 lx) for 15 mins to 5 hours. In all groups, immediately before the MRI experiment, animals were anesthetized with urethane (36% solution intraperitoneally; 0.083 mL / 20 g animal weight, prepared fresh daily; Sigma–Aldrich, St. Louis, MO, USA) and treated topically with 1% atropine to ensure dilation of the iris during light exposure followed by 3.5% lidocaine gel to reduce eye motion. MRI data were acquired using several single spin-echo sequences (time to echo 13 ms, 7×7 mm^2, matrix size 160×320, slice thickness 600 μm). Images were acquired at different repetition times (TR) in the following order (number per time between repetitions in parentheses): TR 0.15 seconds (6), 3.50 seconds (1), 1.00 seconds (2), 1.90 seconds (1), 0.35 seconds (4), 2.70 seconds (1), 0.25 seconds (5), and 0.50 seconds (3). To compensate for reduced signal–noise ratios at shorter TRs, progressively more images were collected as the TR decreased. The present resolution in the central retina is sufficient for extracting meaningful layer-specific anatomical and functional data, as previously discussed [37].

T1 data sets were collected from different groups of mice given an intraperitoneal injection of 29 mg/kg sildenafil, a dose that produces a transient impairment in retinal electrophysiology [12]. This dose is expected to produce a plasma level of sildenafil that is less than 2x that reported in humans [9]. In all cases, sildenafil was administered 45 min– 1 hr 15 min (i.e., ~1 hr) before QUEST MRI examination.

All mice were treated 24 hrs prior to study with 1 mg/kg MB (i.p., dissolved in saline) and then treated the next day with 29 mg/kg sildenafil ~1 h before the MRI examination. 50 mg/kg ALA (i.p., dissolved in saline and pH adjusted to ~7.4) was given 15–20 minutes post-sildenafil injection. Control mice were also given sildenafil as above but administered two saline

injections rather than MB and ALA. The MB and ALA combination has been confirmed to suppress the excessive production of free radicals in several studies [20, 28, 32, 33].

MRI data analysis

As previously described, for QUEST data, each T1 data set of 23 images was first processed by registering (rigid body; STACKREG plugin, ImageJ, Rasband, W.S., ImageJ, U. S. National Institutes of Health, Bethesda, Maryland, USA, https://imagej.nih.gov/ij/, 1997–2016) and then averaging images with the same TRs in order to generate a stack of 8 images [20, 28, 32, 33]. These averaged images were then registered (rigid body) across TRs. QUEST data were corrected for imperfect slice profile bias in the estimate of T1, as previously described (Chapter 18 in [38]). Briefly, by normalizing to the shorter TR, some of the bias can be reduced, giving a more precise estimate for T1. To achieve this normalization, we first apply a 3x3 Gaussian smoothing (performed three times) on only the TR 150 ms image to minimize noise and emphasize signal. The smoothed TR 150 ms image was then divided into the rest of the images in that T1 data set. Previously, we reported that this procedure helps to minimize day-to-day variation in the 1/T1 profile previously noted and obviated the need for a "vanilla control" group used previously for correcting for day-to-day variations [39, 40]. 1/T1 maps were calculated using the 7 normalized images via fitting to a three-parameter T1 equation ($y = a + b^{*}$ (exp(-c*TR)), where a, b, and c are fitted parameters) on a pixel-by-pixel basis using R (v.2.9.0, R Development Core Team [2009]). R: A language and environment for statistical computing. R Foundation for Statistical Computing, Vienna, Austria. ISBN 3–900051–07–0) scripts developed in-house, and the minpack.lm package (v.1.1.1, Timur V. Elzhov and Katharine M. Mullen minpack.lm: R interface to the Levenberg-Marquardt nonlinear least-squares algorithm found in MINPACK. R package version 1.1–1).

In each mouse, whole retinal thicknesses (μm) were objectively determined using the "half-height method" wherein a border is determined via a computer algorithm based on the crossing point at the midpoint between the local minimum and maximum, as detailed elsewhere [41, 42]. The distance between two neighboring crossing-points thus represents an objectively defined retinal thickness. 1/T1 profiles in each mouse were then normalized with 0% depth at the presumptive vitreoretinal border and 100% depth at the presumptive retina-choroid border. The present resolution is sufficient for extracting meaningful layer-specific anatomical and functional data, as previously discussed [43, 44].

We compared superior and inferior profiles separately from ± 400 to 1000 μm (central retina) and ± 1000 to 2000 μm (peripheral retina) from the optic nerve head (ONH) generated for each animal group (Fig 1). Excessive and asynchronous production of paramagnetic free radicals in retinal laminae is measured based on a reduction in 1/T1 with MB and ALA (i.e., a positive QUEST MRI response) [29]. However, an increase in 1/T1 in response to MB or ALA has no theoretical or biophysical basis linking it with oxidative stress. Thus, only significant decreases in 1/T1 following anti-oxidants are indicated on the graphs.

DCF map *ex vivo* of steady-state levels of reactive oxygen species

The net result of production of reactive oxygen species (i.e., free radicals and H_2O_2) minus their elimination by endogenous antioxidants was mapped for each retina using a standard and well validated DCF assay [34, 45]. The interaction of the non-fluorescent probe 2',7'-dichlorodihydrofluorescein (DCFH(2)) produces a fluorescent signal from its oxidation product, 2',7'-dichlorofluorescein (DCF), that represents steady state levels of total reactive oxygen species [46]. DCF measurements were performed in subgroups of mice maintained in darkness for at least 16 hrs before euthanasia. The following day, light adaptation began for all mice
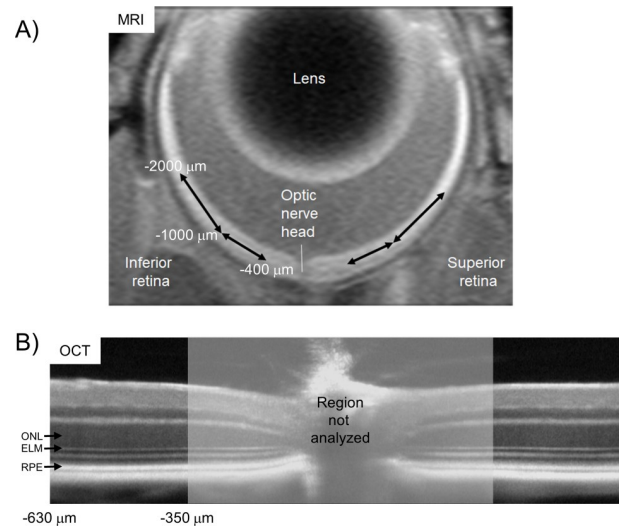
Fig 1. Comparison of MRI and OCT regions-of-interest (ROI's). Four non-overlapping retinal regions were evaluated from MRI data A): ± 400–1000 μm and ± 1000–2000 μm from the optic nerve head for their transretinal 1/ T1 profiles (shown in Figs 3 and 6). Two regions in central retina were studied from OCT data B): ± 350–630 μm from the optic nerve head to determine outer nuclear layer (ONL) thickness, and the external limiting membrane–retinal pigment epithelium (ELM-RPE) thickness.

https://doi.org/10.1371/journal.pone.0245161.g001

at the same time; each mouse experienced between 30 min and 3 hour of room light. 1 hr before enucleation, mice (n = 3 / group) were given 29 mg/kg sildenafil or equal volume saline; dark-adapted mice were not examined since neither QUEST MRI nor QUEST OCT studies suggested oxidative stress in that group.

In all cases, eyes were enucleated and embedded in optimal cutting temperature compound and fresh frozen using liquid nitrogen vapor. DCF staining was conducted as previously reported [47]. Twelve microns sections were cut in vertical (inferior-superior) orientation, and while still frozen, sections were fixed in ice cold acetone at -80°C. Slides were then warmed to room temperature for at least 20 minutes. Section were washed in PBS 3 times in 5 minutes. Slides were transferred in humidified chamber, and sections were submerged in 10 μM DCF (D6883, Sigma-Aldrich Corp., St Louis, MO), and incubated at 37°C for 1 hour. Sections were then washed in PBS 3 times in 5 minutes, and one time in distilled water, cover-slipped using ProLong Gold anti-fade reagent with the nuclear stain 4′,6-diamidino-2-phenylindole (DAPI, P36935; Invitrogen, Carlsbad, CA, USA), and images taken by fluorescence microscopy (Keyence BZ-800 Series; Itasca, IL, USA) immediately after putting on the cover slip.

QUEST optical coherence tomography (QUEST OCT)

Five groups were studied using QUEST OCT as previously described [24]. 1.) Light-adapted control mice: Age-matched C57BL/6 mice dark-adapted overnight and room light-adapted (~300 lx) for 5 hrs the following day, no injections beyond anesthesia. 2.) Dark-adapted control mice: Age-matched C57BL/6 mice dark-adapted overnight and studied in the dark the following day, no injections beyond anesthesia. For the remaining three groups, MB or saline are administered ~24 hr before the study and ALA or saline given 15–20 minutes after the sildenafil. 3.) For this group, Sildenafil is administered after 4 hr of room Light and studied 1 hr later in the Light (SLL, Fig 2A). 4.) For this group, Sildenafil is given in the Dark, then Light-adapted and studied 5 hr later (SDL, Fig 2B). 5.) For this group, Sildenafil is given in the Dark and studied 1 hr later in the Dark (SDD, Fig 2C).
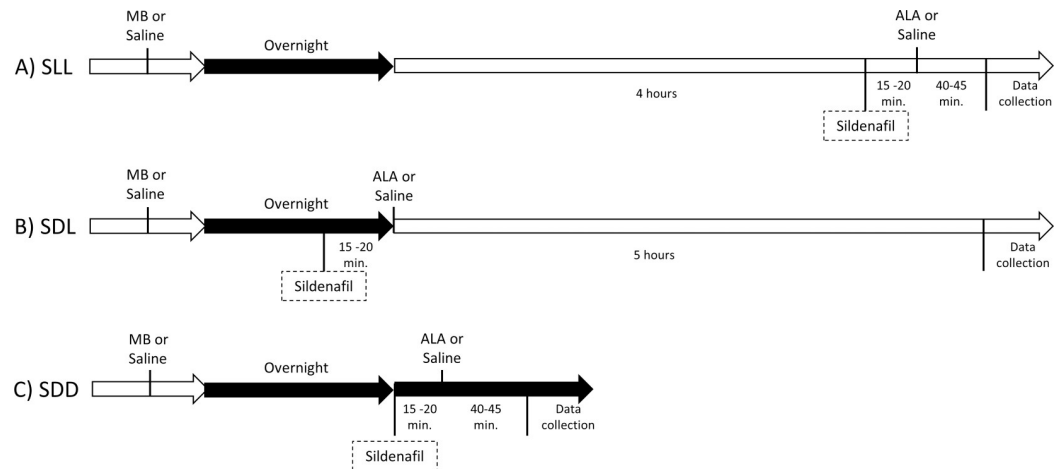
Fig 2. Timing diagrams for the three groups studied by OCT. A) <u>S</u>ildenafil is administered after 4 hr of room <u>L</u>ight and studied 1 hr later in the <u>L</u>ight (SLL). B) <u>S</u>ildenafil is given in the <u>D</u>ark then <u>L</u>ight-adapted and studied 5 hr later (SDL). C) <u>S</u>ildenafil is given in the <u>D</u>ark and maintained as <u>D</u>ark-adapted during OCT examination (SDD). MB, methelyene blue; ALA; α-lipoic acid. Control groups were given saline.

In all groups, OCT (Envisu R2200 VHR SDOIS) was used to measure retinal layer spacing *in vivo*. Mice were anesthetized with urethane (36% solution intraperitoneally; 0.083 ml/20 g animal weight, prepared fresh weekly; Sigma-Aldrich, St. Louis, MO). 1% atropine sulfate was used to dilate the iris, and Systane Ultra was used to lubricate the eyes. Vertical B scan OCT was used in two ways. The first use is to identify retinal layers that contribute to the superior-inferior MRI profile data since aligning the vitreous-retina (0% depth) and retina-choroid (100% depth) borders of OCT and MRI images reasonably matches structure with function [25]. Second, separate groups of mice were studied in which the optic nerve is positioned to interrogate i) central, superior, and inferior retina (± 350–630 μm, Fig 1), ii) inferior retina (350–1191 μm), and iii) superior retina (350–1191 μm) [48]. The ELM-RPE and ONL thicknesses were measured using in-house developed R scripts that objectively identify layer boundaries after searching the space provided by a hand-drawn estimate ("seed boundaries").

QUEST optokinetic tracking (QUEST OKT)

As previously described, QUEST OKT was performed in separate experiments [20]. Four groups of mice were studied (only data collected before 12 pm are reported herein): 1.) Control group: Age-matched C57BL/6 mice, dark-adapted overnight and light-adapted for 5 hrs the following day, no injections beyond anesthesia. 2.) SLL group ± MB / ALA. 3.) SDL group ± MB / ALA. 4.) To see if visual performance recovers to baseline, we also examined a SLL 24 hr recovery group ± MB / ALA: In this group, light-adapted mice were given 29 mg/kg of sildenafil followed by 1 mg/kg MB or equal volume saline an hour later. Mice were dark-adapted overnight then given 50 mg/kg ALA or equal volume saline, brought into the light for 5 hours and studied by OKT.

For all groups, two cone-based visual performance metrics were evaluated in awake and freely moving mice using optokinetic tracking: spatial frequency thresholds (SFTs, "acuity", in cycles/degree [c/d]) and contrast sensitivity (CS, measured near the peak of the nominal curve [0.06 cycles/degree [49]], inverse Michelson contrast [unitless]) (OptoMotry, CerebralMechanics Inc, Alberta, Canada). In brief, a vertical sine wave grating is projected as a virtual cylinder in 3-dimensional coordinate space on computer monitors arranged in a quadrangle around a

testing arena. Unrestrained mice (as described above) are placed on an elevated platform at the center of the arena. An experimenter observed a video image of the platform from above to view the animal and follow the position of its head with the aid of a computer mouse and a crosshair continually placed on the mouse head as it moves. The X–Y positional coordinates of the crosshair are centered on the hub of the virtual cylinder, enabling its wall to be maintained at a constant "distance" from the animal's eyes, and thereby fixing the spatial frequency of the stimulus at the animal's viewing position. When the cylinder was rotated in the clockwise or counter-clockwise direction and the animal followed with head and neck movements that tracked the rotation, it was judged whether the animal's visual system could distinguish the grating. Clockwise and counterclockwise tracking provide a measure of left and right eye SFT and CS [50]. After being in the light for 5 hrs, each set of SFT and peak of CS measurements per mouse can reliably be obtained in 30 minutes. Rod-based visual performance indices evaluated with OKT have limited dynamic range and were not considered to be useful for testing for impairment by oxidative stress [51].

Statistical analysis

Data are presented as mean ± 95% confidence interval, and a significance level of 0.05 was used for all analyses. All outcomes (1/T1, OCT layer thickness, and OKT) had repeated measures for each mouse. As such, we used mixed models to analyze all outcomes using the Kenward-Roger method for calculating degrees of freedom in Proc Mixed and Proc Glimmix of SAS 9.4 (SAS software, Cary, NC, USA). For the MRI profile data (1/T1) and OCT layer thickness, we used cubic splines to model and compare mouse-specific profiles between groups. We used the same modeling strategy for both 1/T1 and OCT layer thickness. The number of "windows" (i.e., "knots") with a relationship between outcome (1/T1, ELM-RPE thickness, or ONL thickness) and location (depth for MRI, distance from ONH for OCT layer thickness) was initially evaluated separately for each group for any given analysis, and the Akaike and Schwarz Bayesian information criteria (AIC and BIC) were used to identify the model with the fewest knots needed to model all groups. These initial models included full fixed effects (described separately for 1/T1 and OCT thickness below) and included a random intercept for each mouse nested within the appropriate treatment group. Additional random coefficients for side (indicator variable for superior side), region (indicator of 1000–2000 μm region), and location-specific coefficients (cubic spline coefficients) were evaluated using AIC and BIC. These models with the selected number of knots and random effects were then used to test for the fixed effects for each model, and non-significant interactions were removed to obtain the final model. The final model was then used to estimate mean profiles for all experimental conditions, and location-specific mean differences based on appropriate contrasts.

For 1/T1, each mouse was measured at 26 depths on two sides in two regions, resulting in 104 observations per mouse. We used Proc Mixed to fit the model for 1/T1, which included seven knots and the fixed effects for anti-oxidant (saline vs MB/ALA), side (inferior vs superior), condition (dark vs light), region (400–1000 μm vs 1000–2000 μm), as well as all interactions among these fixed effects and the locations. The final model included the random coefficients for side; region; linear relationship with depth; the fourth knot coefficient; all two-way interactions among side, region, and the fourth knot coefficient; and the interaction between region and the linear relationship with depth. The parameter estimates for the model are shown in S1 and S2 Tables in S5 File. The analysis of 1/T1 focused on identifying the depths at which an MB/ALA effect was statistically significant using pointwise hypothesis testing only when interactions were significant.

Table 1. Model details for OCT layer thickness analysis.

Outcome	Position relative to ONH	Number of Knots	Random Coefficients
ELM-RPE thickness	Inferior	9	Intercept, Knot 7
	Superior	10	Intercept, Knot 7, Knot 8
ONL thickness	Inferior	7	Intercept, Knot 5
	Superior	9	Intercept, Knot 7

https://doi.org/10.1371/journal.pone.0245161.t001

For the OCT data, each mouse was measured at 720 distances from the ONH on both sides of the ONH. We used Proc Glimmix to fit four models to the OCT data, a separate model for each outcome (changes in ELM-RPE or ONL) and for inferior and superior sides. All models included fixed effects for group (light-adapted control, CL; dark-adapted control, CD; SLL; SLL+MB/ALA; SDL; SDL+MB/ALA; SDD, SDD+MB/ALA), values for the spline coefficients for the distance from the ONH and the interaction between distance from the ONH and group. The number of knots and random coefficients used for the final models are shown in Table 1. The parameter estimates for these models are shown in S3–S10 Tables in S5 File. Contrasts were used with each final model to calculate a mean integrated across the entire layer. These contrasts were also used to compare the integrated means among the groups. We compared each group to the both controls and MB/ALA was compared only within a group (e.g., SLL vs SLL+MB/ALA). We used the Holm procedure to adjust for multiple comparisons for each focal group (SLL, SDL, and SDD).

OKT was measured once per side, resulting in only two observations per mouse. As such, we used generalized linear mixed models (Proc Glimmix) to analyze both OKT measurements. For both acuity and contrast sensitivity, we included the fixed effect of group (saline, SLL, SLL+MB/ALA, SDL, SDL+MB/ALA, 24hr, 24hr+MB/ALA. Only a random intercept for mouse nested within group was included for these models. We used a normal distribution with the identity link for acuity and a gamma distribution with the log link for contrast sensitivity. The parameter estimates for the fit models are shown in S13–S16 Tables in S5 File. As with OCT distances, we compared each experimental group to saline, and compared the MB/ALA treatment within a focal group. We used the Holm procedure to adjust for multiple comparisons.

Results

Testing light-adapted mouse rods for oxidative stress 1 hr post-sildenafil (SLL)

QUEST MRI. As shown in Fig 3 (see S1 Fig in S5 File for raw data), significant ($p < 0.05$) evidence for oxidative stress was found to be limited to the peripheral (i.e., 1000–2000 μm from the ONH) retina on the superior side (i.e., Fig 3B). Central (± 400–1000 μm) retina and peripheral inferior outer retina did not show evidence for oxidative stress ($p > 0.05$, Fig 3).

DCF. A representative data set showing steady state levels of reactive oxygen species evaluated by DCF staining in freshly isolated retinal sections is shown in Fig 4. In saline treated mice, little DCF fluorescence was noted ("saline" row, Fig 4). In sildenafil treated mice, DCF signal was seen prominently in the superior peripheral outer retina (top row, Fig 4) with less signal observed in the inferior retina.

QUEST OCT. In untreated control mice, superior and inferior central ELM-RPE was significantly ($p < 0.05$) ~5 μm thinner in the dark than after 5 hr of light-adaptation (Fig 5, and S3 Fig in S5 File for raw data), a similar effect size as previously reported using a higher spatial resolution OCT [52]. Light-dark data collected before 12:30 pm are reported herein. In the
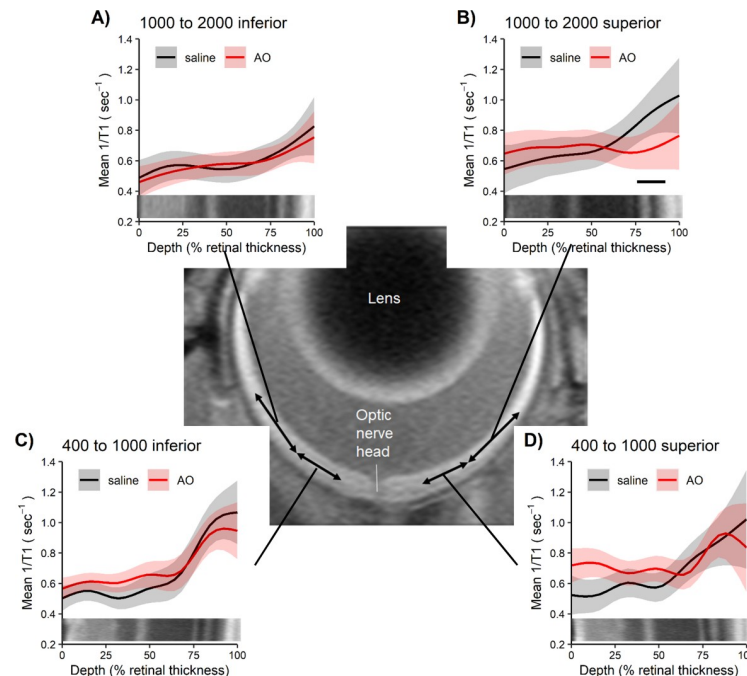
Fig 3. QUEST MRI showing oxidative stress localized to peripheral superior retina. Modeled 1/T1 profiles approximately 1 hour post-sildenafil IP in light-adapted mice given either saline (n = 4 mice, black line) or anti-oxidants (AO, n = 5 mice, red line) in these four retinal regions: A) 1000 to 2000 inferior, B) 1000 to 2000 superior, C) 400–1000 inferior, and D) 400–1000 superior; representative OCT images (bottom of each graph) provide spatial orientation. Only significant (horizontal black bar) AO reductions in 1/T1 indicative of oxidative stress are shown. Each profile has a solid line indicating the mean and a shaded region indicating 95% confidence intervals.

central retina (± 350–630 μm from the ONH), sildenafil reduced ($p < 0.05$) the ELM-RPE thickness from light- to dark-adapted levels in control mice (Fig 5); anti-oxidants did not ($p > 0.05$) restore ELM-RPE thickness to light-like values as would be expected if oxidative stress were present [24]. Similar results are found with a field-of-view ± 350–1191 μm from the optic nerve head (S4 Fig in S5 File).

In contrast to the ELM-RPE region, ONL was, as expected, invariant in dark and light-adapted control mice, and following administration of sildenafil (Fig 5 for ± 350–630 μm from the optic nerve head; ± 350–1191 μm from the optic nerve head data are shown in S4 Fig in S5 File) [44, 54].

Testing light-adapted mouse for outer retina oxidative stress 5 hr post-sildenafil (SDL)

QUEST OCT. 5 hr after sildenafil administration, the ELM-RPE thickness in the central retina (± 350–630 μm from the optic nerve head) was not different ($p > 0.05$) from light-adapted levels of control mice and thicker than dark-adapted levels (Fig 6 and S5 Fig in S5 File for raw data); again, anti-oxidants had no effect ($p > 0.05$) in the sildenafil-treated mice (Fig 6 and S5 Fig in S5 File for the raw data) [24]. Results with a field-of-view ± 350–1191 μm from the optic nerve head (S6 Fig in S5 File) are consistent with the central retina findings.

ONL thickness was invariant ($p > 0.05$) to sildenafil or anti-oxidants (Fig 6 for ± 350–630 μm from the optic nerve head; ± 350–1191 μm from the optic nerve head data are shown in S6 Fig in S5 File), supporting a specific sildenafil response by the ELM-RPE region.
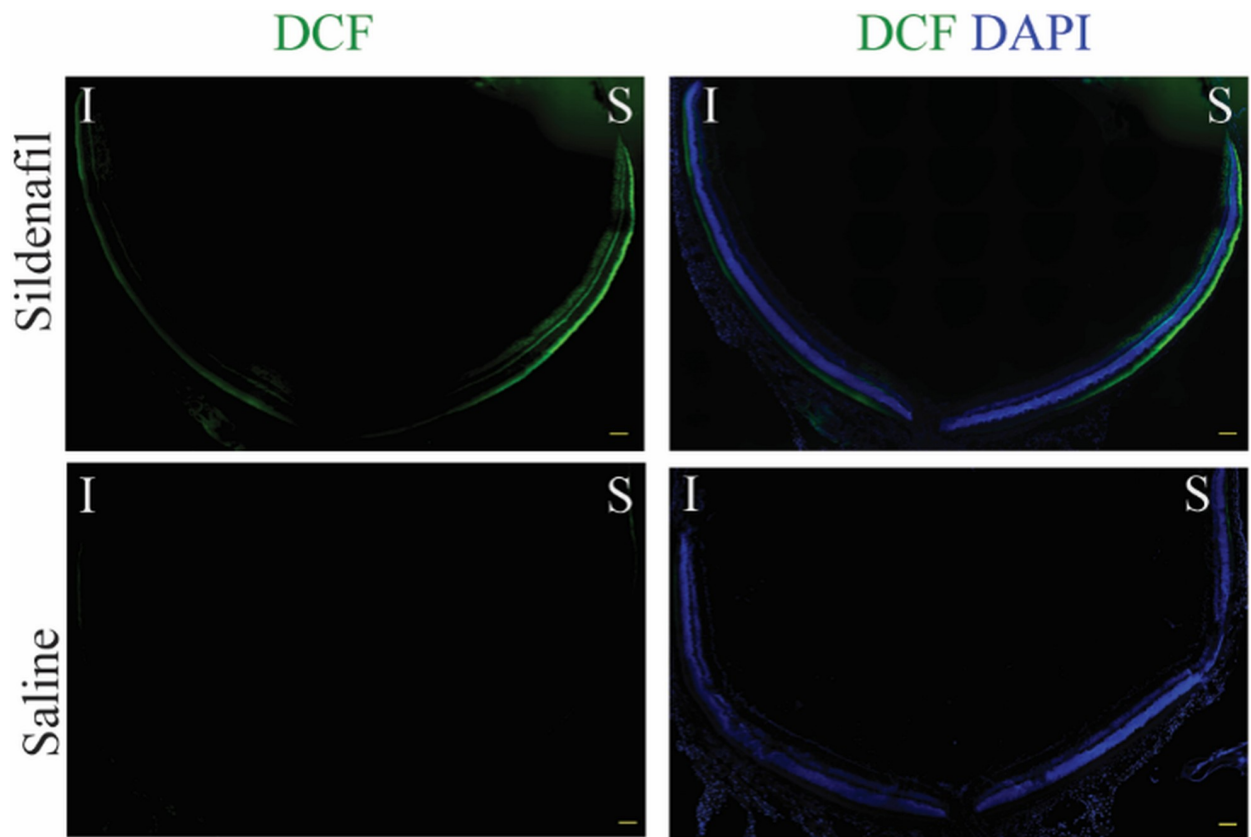
Fig 4. The effect of sildenafil on generation of oxidative stress in a representative *ex vivo* data set of unfixed cryosections stained with DCF. DCF staining for reactive oxygen species is shown in green; nuclei staining (DAPI) is shown in blue. The same intensity scaling is used in all images; scale bars are 100 μm.

https://doi.org/10.1371/journal.pone.0245161.g004

Testing dark-adapted mouse for outer retina oxidative stress 1 hr post-sildenafil (SDD)

QUEST MRI. No evidence (p > 0.05) for oxidative stress was found in superior or inferior dark-adapted retina in any layers (Fig 7 and S7 Fig in S5 File for raw data). For completeness, we note that the inferior inner retina (0–24% depth) did show evidence (p < 0.05) for oxidative stress (i.e., Fig 7C).

QUEST OCT. In the dark, the ELM-RPE thickness in the central retina (± 350–630 μm from the optic nerve head) was not different (p > 0.05) from dark-adapted levels of control mice and was thinner, as expected, than light-adapted levels independent of administration of anti-oxidants (Fig 8 and S8 Fig in S5 File for raw data) [24]. Comparable outcomes were observed with a field-of-view ± 350–1191 μm from the optic nerve head (S9 Fig in S5 File).

In addition, the ONL thickness was constant regardless of treatment with sildenafil or anti-oxidants (Fig 8 for ± 350–630 μm from the optic nerve head; ± 350–1191 μm from the optic nerve head shown in S9 Fig in S5 File).

Testing visual performance 1, 5, and 24 hr post-sildenafil

QUEST OKT. At 5 hr post-sildenafil treatment, CS was lower-than-normal (p < 0.05) and not corrected by anti-oxidants (Fig 9). No change (p > 0.05) in CS from control values was noted at 1 hr or 24 post-sildenafil. SFT was unaffected by both sildenafil ± anti-oxidants in all groups (Fig 9).
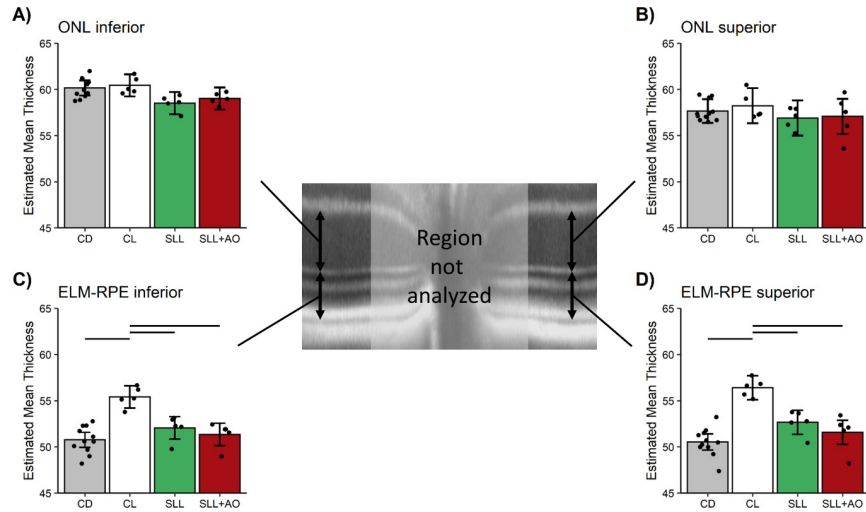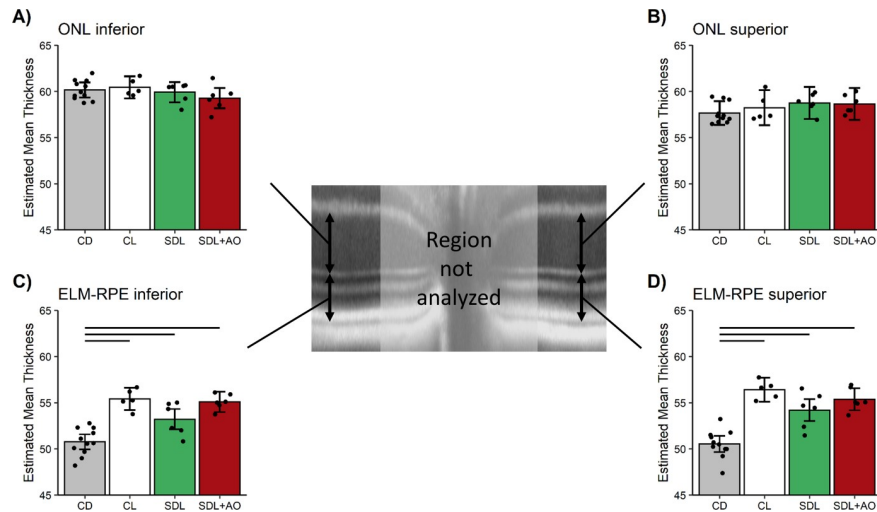
Fig 5. 1 hr post-sildenafil after 4 hr of light-adaption mice (SLL, Fig 2) shows thinner, dark-like ELM-RPE.
Modeled A) ONL inferior retina, B) ONL superior retina, C) ELM-RPE thickness inferior retina, and D) ELM-RPE thickness superior retina in uninjected control dark (CD, n = 11 mice, grey bar), control light (CL, n = 5 mice, white bar), SLL+saline (SLL, n = 5 mice, green bar), and SLL+AO (n = 5 mice, red bar) in the two different retinal regions. ONL is invariant to condition. ELM-RPE is significantly (horizontal black bar) thinner in the dark than in the light (CD vs. CL) as expected [44, 53, 54]. In SLL+saline and SLL+AO groups ELM-RPE thickness is not different from CD (and was thinner than CL); no evidence for oxidative stress was found. The points in each plot represent the estimated mean for each mouse based on the model. Error bars indicate 95% confidence intervals. Note the same control data sets are presented in each graph to facilitate comparisons.

Discussion

In this study, we find evidence for a spatially limited oxidative stress response to sildenafil, and that sildenafil-impaired vision cannot be rescued by AO. Therefore, it is likely that sildenafil-

Fig 6. 5 hr post-sildenafil in light-adaption mice (SDL, Fig 2) shows light-like ELM-RPE. Modeled A) ONL inferior retina, B) ONL superior retina, C) ELM-RPE thickness inferior retina, and D) ELM-RPE thickness superior retina in uninjected control dark (CD, n = 11 mice, grey bar), control light (CL, n = 5 mice, white bar), SDL+saline (SDL, n = 6 mice, green bar), and SDL+AO (n = 6 mice, red bar) in the two different retinal regions. ONL is unresponsive to condition. In SDL+saline and SDL+AO groups ELM-RPE thickness is not different from CL (and was thicker than CD); no evidence for oxidative stress was found. The points in each plot represent the estimated mean for each mouse based on the model. Error bars indicate 95% confidence intervals. Note the same control bars are presented in each graph to facilitate comparisons.
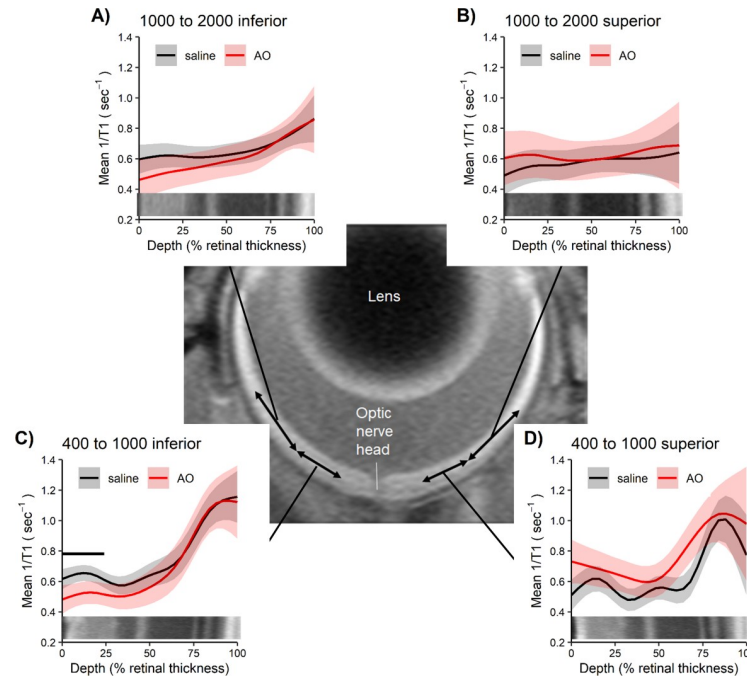
Fig 7. QUEST MRI in dark-adapted mice do not show outer oxidative stress. Modelled 1/T1 profiles approximately 1 hour post-sildenafil IP in dark-adapted mice given either saline (n = 6 mice, black line) or anti-oxidants (AO, n = 3 mice, red line) in these four retinal regions: A) 1000 to 2000 inferior, B) 1000 to 2000 superior, C) 400–1000 inferior, and D) 400–1000 superior; representative OCT images (bottom of each graph) provide spatial orientation. Only significant (horizontal black bar) AO reduction in 1/T1 indicative of oxidative stress are shown. Each profile has a solid line indicating the mean and a shaded region indicating 95% confidence intervals.
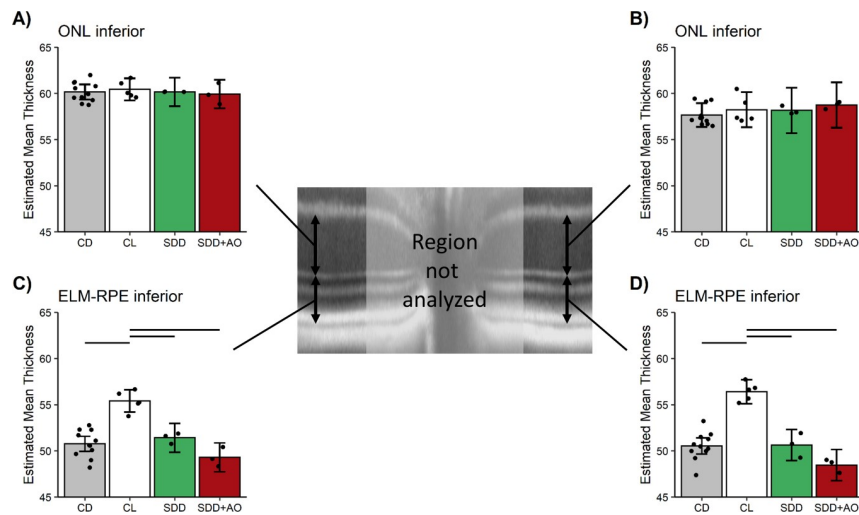
https://doi.org/10.1371/journal.pone.0245161.g007

Fig 8. 1 hr post-sildenafil in dark-adapted mice (SDD, Fig 2) shows thinner ELM-RPE. Modeled A) ONL inferior retina, B) ONL superior retina, C) ELM-RPE thickness inferior retina, and D) ELM-RPE thickness superior retina in uninjected control dark (CD, n = 11 mice, grey bar), control light (CL, n = 5 mice, white bar), SDD+saline (SDD, n = 3 mice, green bar), and SDD+AO (n = 3 mice, red bar) in the two different retinal regions. ONL is constant regardless of condition. In SDD+saline and SDD+AO groups, ELM-RPE thickness is not different from CD (and was thinner than CL); no evidence for oxidative stress was found. The points in each plot represent the estimated mean for each mouse based on the model. Error bars indicate 95% confidence intervals. Note the same control bars are presented in each graph to facilitate comparisons.

https://doi.org/10.1371/journal.pone.0245161.g008
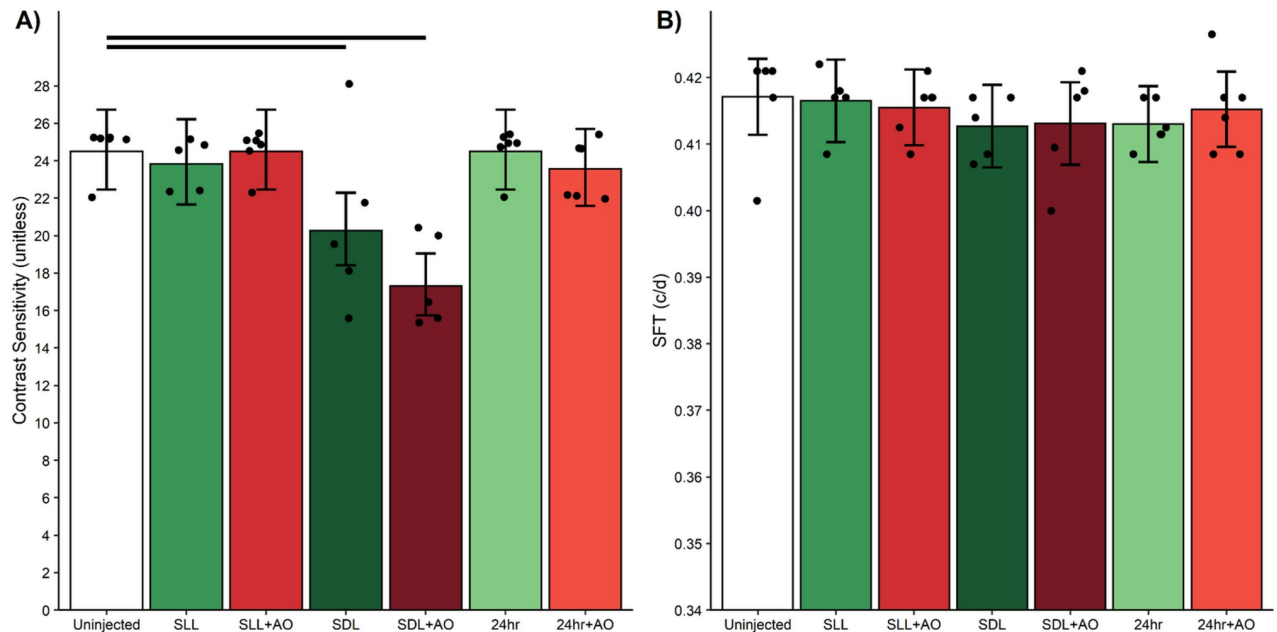
Fig 9. Contrast sensitivity is transiently reduced at 5 hr post-sildenafil. Compared to uninjected 5 hr light adapted mice (white bar), sildenafil + saline (green bars) A) decreased contrast sensitivity only under SDL conditions but B) did not change spatial frequency threshold (SFT). AO (red bars) did not correct this reduced contrast sensitivity. Black horizontal bars indicate significant differences (P < 0.05). The points in each plot represent the estimated mean for each mouse based on the model. Error bars are 95% confidence intervals. Number of mice used per group: uninjected, n = 6 mice; SLL+saline, n = 5 mice; SLL+AO, n = 6 mice; SDL+saline, n = 5 mice; SDL+AO, n = 5 mice; 24 hour+saline, n = 6 mice; 24 hour+AO, n = 6 mice.

induced vision impairment is caused by mechanisms other than oxidative stress, a topic for future study.

Sildenafil and retina oxidative stress

In this study, we found no evidence to support the first part of our hypothesis that systemic sildenafil can cause widespread outer retinal oxidative stress in light-adapted mice (Figs 3 and 4). Unexpectedly, the oxidative stress (as measured by QUEST MRI *in vivo* and DCF *ex vivo*) at 1 hr post-treatment was found most prominently in superior peripheral outer retina (Figs 3 and 4). Intriguingly, we note that other retinal regions (e.g., superior central outer retina) show different oxidative stress results by QUEST MRI and DCF. These different spatial outcomes do not appear to be due to different detection sensitivities because, for example, a third method, QUEST OCT, did not show evidence for oxidative stress in inferior or superior central retina (Fig 5). Alternatively, we note that QUEST MRI detects paramagnetic free radicals and is unable to detect non-paramagnetic species like H_2O_2. However, DCF detects both free radicals and H_2O_2 [45]. We also note that QUEST OCT detects high levels of superoxide but its sensitivity to other reactive oxygen species is unknown [20, 24, 44]. More work is needed to unravel which reactive oxygen species contribute to the positive QUEST MRI, DCF, and QUEST OCT results.

Regionally specific oxidative stress has been reported in PDE 6 mutant rd10 mice and in other models [31, 33, 55–57]. We note that non-invasive measures of oxidative stress measured by QUEST MRI, QUEST OCT, and QUEST OKT are only revealed with AO injection, and the use of saline controls is thus better than un-injected controls. The present results are consistent with the notion that seemingly homogeneous population of neurons (in this case rod

photoreceptors) can have substantial within-class heterogeneity [55]. Limitations of the present study include not considering sex and age, two important biological variables; more work is now needed in female and older mice.

As noted above, QUEST OCT found no evidence for oxidative stress in the ELM-PRE region of the central retina [24, 29, 33]. QUEST OCT relies on the fact that oxidative stress causes a thinner, dark-like ELM-RPE thickness even in the light, perhaps due to induced acidosis [58–60]. This phenotype comes about because the ELM-RPE thickness is modulated by a signaling pathway in which rod photoreceptor cells consume more energy in the dark than in the light [26, 27, 32, 44, 61, 62]. As a result, there is a greater production of waste-water and CO_2 that acidifies the subretinal space [26, 27, 32, 44, 61, 62]. In turn, this causes an upregulation of pH-sensitive water-removal co-transporters on the apical portion of the RPE (Fig 10) [26, 27, 32, 44, 61, 62]. Thus, oxidative stress is indicated if in light-adapted mice, anti-oxidants convert a dark-like thin subretinal space into a thicker light-like level (Fig 10), an outcome not found in this study (Figs 5, 6, 8) [24].

Mechanistically, the evoked oxidative stress at 1 hr post-treatment (at the presumptive peak of plasma sildenafil and associated cGMP content) is hypothesized to occur via focal inhibition of photoreceptor PDE 6 activity [12]. In this scenario (summarized in Fig 10), elevating cGMP levels in light-adapted mice causes sustained opening of rod photoreceptor outer segment cyclic nucleotide-gated channels, an energy-intensive event [64]. As a result of this increase in mitochondrial respiration, the subretinal space fills with acidified waste-water [14, 17–19, 24, 28, 65]. The lowering of the subretinal space pH upregulates water removal co-transporters in RPE with the end result of dehydrating / thinning of the ELM-RPE space (Fig 10) [14, 17–19, 24, 28, 65]. Evidence for subretinal space thinning following sildenafil is shown in Fig 3 [14, 17–19, 24, 28, 65]. The associated increase in mitochondrial activity can cause production of free radicals in excess of anti-oxidant defenses [16]. The above may also provide a possible explanation for the oxidative stress measured in the inferior inner central retina (a PDE 5-rich region) of dark-adapted mice (Figs 4 and 6) [7, 12, 66]. While sustained cGMP content can cause photoreceptor cell death, the induced focal oxidative stress in this study (Fig 3) appears to be non-toxic since visual performance was normal 24 hours after the sildenafil treatment [16–19, 31, 65, 67]. Since the outer retina is avascular, the focal oxidative stress in posterior retina is unrelated to a sildenafil effect on endothelial cells [68]. There are reports, however, in non-retinal disease models that chronic treatment with sildenafil shows anti-oxidant effects [69, 70]. More work is needed to understand the events leading to the localized oxidative stress *in vivo* measured in the present investigation.

Sildenafil and visual performance

We further found novel evidence that sildenafil can temporarily impair contrast sensitivity but not spatial frequency thresholds (i.e., acuity) in healthy C57BL/6 mice (Fig 9). This visual performance decline in response to sildenafil was not corrected with anti-oxidants, suggesting a non-oxidative stress etiology. The transient nature of the response (Fig 9) may help understand why sildenafil's effect on retinal electrophysiologic indices from experimental models has been contradictory [6–9, 12, 13].

Intriguingly, the induced visual performance declines also did not seem linked with higher rod cGMP levels. In particular, sildenafil's plasma concentration peaks at about 1 hr post-injection followed by clearance with a half-life of ~4 hr; effects on retinal electrophysiology are reported to be gone by 24 hr post-injection [6, 12, 66, 71]. Sildenafil's content in the retina is ~2-fold higher than in the plasma and so the resulting higher retinal cGMP levels are expected to follow a similar time course as sildenafil in the plasma [9]. Indeed, in this study, a smaller
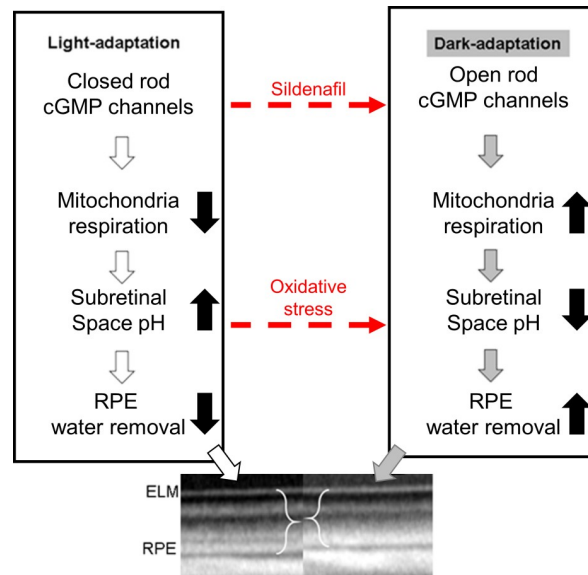
Fig 10. Working model of factors that regulate the ELM-RPE thickness. Oxidative stress is hypothesized to induce an acidosis (dotted red line) that would be expected to convert a thicker "light" ELM-RPE phenotype into a thinner "dark-like" phenotype (see text for details); this expectation is supported experimentally [24, 44, 63].

https://doi.org/10.1371/journal.pone.0245161.g010

rod ELM-RPE thickness was evident at 1 hr post-sildenafil with recovery to thicker light-like levels by 5 hr (Fig 5) in-line with the expected changes in cGMP levels (Fig 10) [6, 9, 12, 66, 71]. However, contrast sensitivity was normal at 1 hr post-sildenafil (i.e., at the presumptive maximum plasma and retinal levels of sildenafil and cGMP, respectively) (Fig 9) [12]. On the other hand, visual performance was lowest at 5 hr post-treatment (i.e., when levels are roughly at half-maximum) (Fig 9) [12]. The present data are insufficient to explain the temporal mismatch between lower contrast sensitivity and rod cGMP levels, especially since cones are more sensitive to sildenafil inhibition than rods [12]. Additional studies are needed to investigate whether, for example, this mismatch has contributions from retinal sildenafil P450 metabolism or from PDE inhibition in other parts of the brain [10, 72–74].

Summary

Sildenafil induced spatially localized photoreceptor oxidative stress based on i) the QUEST MRI and DCF data showing prominent signal from superior peripheral outer retina dominated by rods in the light demonstrating oxidative stress [75], ii) the lack of evidence for oxidative stress in central outer retina as measured by QUEST OCT, and iii) lack of anti-oxidant response on OKT cone-based visual performance testing. Thus, we find no evidence for sildenafil-induced oxidative stress in rods panretinally nor was oxidative stress related to sildenafil-induced impairment of visual performance in wildtype mice. In addition, the present findings do not support a role for loss-of-function in PDE 6 *per se* as causative for oxidative stress in dark-reared rd10 mice stress [31]. A novel observation from this study is that ELM-RPE thickness appears to be an indicator of cGMP level changes at least following sildenafil administration; conventional cGMP assays reflect whole retina levels rather than that in the ELM-RPE [76]. This observation might thus address the need for novel cGMP imaging biomarkers in, for example, hereditary photoreceptor degeneration disease, age-related macular degeneration, and neurodegenerative diseases, such as Alzheimer's disease [2, 4, 77].

Supporting information

S1 File. Supplement File. The supplement file contains additional details about the statistical methods used, supplemental tables, supplemental figures, and code for all analyses.
(ZIP)

S2 File. Data for Figs 3 and 7. This file contains the summary data and code needed to generate Figs 3 and 7.
(ZIP)

S3 File. Data for Figs 5, 6, and 8. This file contains the summary data and code needed to generate Figs 5, 6 and 8.
(ZIP)

S4 File. Data for Fig 9. This file contains the summary data and code needed to generate Fig 9.
(ZIP)

S5 File.
(DOCX)

Author Contributions

Conceptualization: Bruce A. Berkowitz, Haohua Qian.

Data curation: Bruce A. Berkowitz.

Formal analysis: Bruce A. Berkowitz, Robert H. Podolsky, Karen Lins Childers, Aicha Saadane.

Funding acquisition: Bruce A. Berkowitz, Timothy S. Kern, Haohua Qian.

Investigation: Aicha Saadane, Robin Roberts, Hailey Olds, Joydip Joy, Collin Richards, Michael Schneider, Brennan Schilling, Arthur Orchanian, Emma Graffice, Kenan Sinan, Lamis Harp.

Methodology: Bruce A. Berkowitz, Robert H. Podolsky.

Project administration: Bruce A. Berkowitz, Timothy S. Kern, Robin Roberts.

Resources: Bruce A. Berkowitz.

Software: Robert H. Podolsky, Tilman Rosales.

Supervision: Bruce A. Berkowitz.

Writing – original draft: Bruce A. Berkowitz, Robert H. Podolsky, Robin Roberts, Haohua Qian.

Writing – review & editing: Bruce A. Berkowitz, Robert H. Podolsky, Timothy S. Kern, Robin Roberts, Hailey Olds, Joydip Joy, Collin Richards, Tilman Rosales, Michael Schneider, Brennan Schilling, Arthur Orchanian, Emma Graffice, Kenan Sinan, Haohua Qian, Lamis Harp.

References

1. Ghiadoni L, Versari D, Taddei S. Phosphodiesterase 5 inhibition in essential hypertension. Current hypertension reports. 2008; 10(1):52–7. Epub 2008/03/28. https://doi.org/10.1007/s11906-008-0011-4 PMID: 18367027.

2. Liu L, Xu H, Ding S, Wang D, Song G, Huang X. Phosphodiesterase 5 inhibitors as novel agents for the treatment of Alzheimer's disease. Brain Res Bull. 2019; 153:223–31. Epub 2019/09/08. https://doi.org/10.1016/j.brainresbull.2019.09.001 PMID: 31493542.

3. Zuccarello E, Acquarone E, Calcagno E, Argyrousi EK, Deng SX, Landry DW, et al. Development of novel phosphodiesterase 5 inhibitors for the therapy of Alzheimer's disease. Biochem Pharmacol. 2020:113818. Epub 2020/01/25. https://doi.org/10.1016/j.bcp.2020.113818 PMID: 31978378.

4. Coleman DJ, Lee W, Chang S, Silverman RH, Lloyd HO, Daly S, et al. Treatment of Macular Degeneration with Sildenafil: Results of a Two-Year Trial. Ophthalmologica. 2018; 240(1):45–54. Epub 2018/04/26. https://doi.org/10.1159/000486105 PMID: 29694963.

5. Barabas P, Riedl Z, Kardos J. Sildenafil, N-desmethyl-sildenafil and Zaprinast enhance photoreceptor response in the isolated rat retina. Neurochem Int. 2003; 43(6):591–5. Epub 2003/06/25. https://doi.org/10.1016/s0197-0186(03)00045-7 PMID: 12820988.

6. Kinoshita J, Iwata N, Shimoda H, Kimotsuki T, Yasuda M. Sildenafil-induced reversible impairment of rod and cone phototransduction in monkeys. Invest Ophthalmol Vis Sci. 2015; 56(1):664–73. Epub 2015/01/13. https://doi.org/10.1167/iovs.14-15985 PMID: 25574056.

7. Martins J, Kolomiets B, Caplette R, Sahel JA, Castelo-Branco M, Ambrosio AF, et al. Sildenafil Acutely Decreases Visual Responses in ON and OFF Retinal Ganglion Cells. Invest Ophthalmol Vis Sci. 2015; 56(4):2639–48. Epub 2015/03/31. https://doi.org/10.1167/iovs.14-15964 PMID: 25814000.

8. Luke M, Luke C, Hescheler J, Schneider T, Sickel W. Effects of phosphodiesterase type 5 inhibitor sildenafil on retinal function in isolated superfused retina. Journal of ocular pharmacology and therapeutics: the official journal of the Association for Ocular Pharmacology and Therapeutics. 2005; 21(4):305–14. Epub 2005/08/25. https://doi.org/10.1089/jop.2005.21.305 PMID: 16117694.

9. Umeya N, Yoshizawa Y, Fukuda K, Ikeda K, Kamada M, Miyawaki I. Availability of multistep light stimulus method for evaluation of visual dysfunctions. J Pharmacol Toxicol Methods. 2019; 96:27–33. Epub 2018/12/26. https://doi.org/10.1016/j.vascn.2018.12.005 PMID: 30583015.

10. Karaarslan C. Ocular Side Effects of Sildenafil That Persist Beyond 24 h—A Case Series. Frontiers in Neurology. 2020; 11(67). https://doi.org/10.3389/fneur.2020.00067 PMID: 32117027

11. Quiram P, Dumars S, Parwar B, Sarraf D. Viagra-associated serous macular detachment. Graefes Arch Clin Exp Ophthalmol. 2005; 243(4):339–44. Epub 2005/03/10. https://doi.org/10.1007/s00417-004-1099-0 PMID: 15756578.

12. Nivison-Smith L, Zhu Y, Whatham A, Bui BV, Fletcher EL, Acosta ML, et al. Sildenafil alters retinal function in mouse carriers of retinitis pigmentosa. Exp Eye Res. 2014; 128:43–56. Epub 2014/09/23. https://doi.org/10.1016/j.exer.2014.08.014 PMID: 25239397.

13. Behn D, Potter MJ. Sildenafil-Mediated Reduction in Retinal Function in Heterozygous Mice Lacking the γ-Subunit of Phosphodiesterase. Investigative Ophthalmology & Visual Science. 2001; 42(2):523–7. PMID: 11157892

14. Zhang X, Feng Q, Cote RH. Efficacy and Selectivity of Phosphodiesterase-Targeted Drugs in Inhibiting Photoreceptor Phosphodiesterase (PDE6) in Retinal Photoreceptors. Investigative Ophthalmology & Visual Science. 2005; 46(9):3060–6. https://doi.org/10.1167/iovs.05-0257 PMID: 16123402

15. Cote RH. Characteristics of photoreceptor PDE (PDE6): similarities and differences to PDE5. International journal of impotence research. 2004; 16 Suppl 1:S28–33. Epub 2004/06/30. https://doi.org/10.1038/sj.ijir.3901212 PMID: 15224133.

16. Sharma AK, Rohrer B. Sustained elevation of intracellular cGMP causes oxidative stress triggering calpain-mediated apoptosis in photoreceptor degeneration. Curr Eye Res. 2007; 32(3):259–69. https://doi.org/10.1080/02713680601161238 PMID: 17453946

17. Martinez-Fernandez de la Camara C, Sequedo MD, Gomez-Pinedo U, Jaijo T, Aller E, Garcia-Tarraga P, et al. Phosphodiesterase inhibition induces retinal degeneration, oxidative stress and inflammation in cone-enriched cultures of porcine retina. Exp Eye Res. 2013; 111:122–33. Epub 2013/04/13. https://doi.org/10.1016/j.exer.2013.03.015 PMID: 23578797.

18. Du Y, Cramer M, Lee CA, Tang J, Muthusamy A, Antonetti DA, et al. Adrenergic and serotonin receptors affect retinal superoxide generation in diabetic mice: relationship to capillary degeneration and permeability. The FASEB Journal. 2015. https://doi.org/10.1096/fj.14-269431 PMID: 25667222

19. Fox DA, Poblenz AT, He L. Calcium overload triggers rod photoreceptor apoptotic cell death in chemical-induced and inherited retinal degenerations. Ann N Y Acad Sci. 1999; 893:282–5. Epub 2000/02/15. https://doi.org/10.1111/j.1749-6632.1999.tb07837.x PMID: 10672249.

20. Berkowitz BA, Podolsky RH, Lenning J, Khetarpal N, Tran C, Wu JY, et al. Sodium Iodate Produces a Strain-Dependent Retinal Oxidative Stress Response Measured In Vivo Using QUEST MRI. Investigative Ophthalmology & Visual Science. 2017; 58(7):3286–93. https://doi.org/10.1167/iovs.17-21850 PMC5493331. PMID: 28666279

21. Patel AK, Hackam AS. A novel protective role for the innate immunity Toll-Like Receptor 3 (TLR3) in the retina via Stat3. Molecular and cellular neurosciences. 2014; 63:38–48. https://doi.org/10.1016/j.mcn.2014.09.004 PMC4250317. PMID: 25264029

22. Cahill H, Nathans J. The optokinetic reflex as a tool for quantitative analyses of nervous system function in mice: application to genetic and drug-induced variation. PLoS ONE. 2008; 3(4):e2055. https://doi.org/10.1371/journal.pone.0002055 PMID: 18446207

23. Jackson CR, Ruan GX, Aseem F, Abey J, Gamble K, Stanwood G, et al. Retinal Dopamine Mediates Multiple Dimensions of Light-Adapted Vision. J Neurosci. 2012; 32(27):9359–68. https://doi.org/10.1523/JNEUROSCI.0711-12.2012 PMID: 22764243

24. Berkowitz BA, Podolsky RH, Lins-Childers KM, Li Y, Qian H. Outer Retinal Oxidative Stress Measured In Vivo Using QUEnch-assiSTed (QUEST) OCT. Invest Ophthalmol Vis Sci. 2019; 60(5):1566–70. Epub 2019/04/18. https://doi.org/10.1167/iovs.18-26164 PMID: 30995313.

25. Berkowitz BA, Bissig D, Roberts R. MRI of rod cell compartment-specific function in disease and treatment in-ávivo. Progress in Retinal and Eye Research. 2016; 51:90–106. https://doi.org/10.1016/j.preteyeres.2015.09.001 PMID: 26344734

26. Adijanto J, Banzon T, Jalickee S, Wang NS, Miller SS. CO2-induced ion and fluid transport in human retinal pigment epithelium. The Journal of General Physiology. 2009; 133(6):603–22. https://doi.org/10.1085/jgp.200810169 PMID: 19468075

27. Wolfensberger TJ, Dmitriev AV, Govardovskii VI. Inhibition of membrane-bound carbonic anhydrase decreases subretinal pH and volume. Doc Ophthalmol. 1999; 97(3–4):261–71. https://doi.org/10.1023/a:1002496223131 PMID: 10896339

28. Berkowitz BA, Bredell BX, Davis C, Samardzija M, Grimm C, Roberts R. Measuring In Vivo Free Radical Production by the Outer Retina. Invest Ophthalmol Vis Sci. 2015; 56(13):7931–8. Epub 2015/12/17. https://doi.org/10.1167/iovs.15-18420 PMID: 26670830; PubMed Central PMCID: PMC4682605.

29. Berkowitz BA. Oxidative stress measured in vivo without an exogenous contrast agent using QUEST MRI. Journal of magnetic resonance (San Diego, Calif: 1997). 2018; 291:94–100. https://doi.org/10.1016/j.jmr.2018.01.013 PMC5963509. PMID: 29705036

30. Berkowitz BA, Podolsky RH, Childers KL, Gow A, Schneider BL, Lloyd SC, et al. Age-related murine hippocampal CA1 laminae oxidative stress measured in vivo by QUEnch-assiSTed (QUEST) MRI: impact of isoflurane anesthesia. GeroScience. 2020. Epub 2020/01/26. https://doi.org/10.1007/s11357-020-00162-8 PMID: 31981008.

31. Berkowitz BA, Podolsky RH, Berri AM, Dernay K, Graffice E, Shafie-Khorassani F, et al. Dark Rearing Does Not Prevent Rod Oxidative Stress In Vivo in Pde6brd10 Mice. Invest Ophthalmol Vis Sci. 2018; 59(3):1659–65. Epub 2018/04/07. https://doi.org/10.1167/iovs.17-22734 PMID: 29625492; PubMed Central PMCID: PMC5868999.

32. Berkowitz BA, Lewin AS, Biswal MR, Bredell BX, Davis C, Roberts R. MRI of Retinal Free Radical Production With Laminar Resolution In Vivo. Invest Ophthalmol Vis Sci. 2016; 57(2):577–85. Epub 2016/02/18. https://doi.org/10.1167/iovs.15-18972 PMID: 26886890; PubMed Central PMCID: PMC4771178.

33. Berkowitz BA, Podolsky RH, Farrell B, Lee H, Trepanier C, Berri AM, et al. D-cis-Diltiazem Can Produce Oxidative Stress in Healthy Depolarized Rods In Vivo. Investigative Ophthalmology & Visual Science. 2018; 59(7):2999–3010. https://doi.org/10.1167/iovs.18-23829 PMID: 30025125

34. Du Y, Veenstra A, Palczewski K, Kern TS. Photoreceptor cells are major contributors to diabetes-induced oxidative stress and local inflammation in the retina. Proceedings of the National Academy of Sciences. 2013; 110(41):16586–91. https://doi.org/10.1073/pnas.1314575110 PMID: 24067647

35. Oz M, Lorke DE, Hasan M, Petroianu GA. Cellular and molecular actions of Methylene Blue in the nervous system. Med Res Rev. 2011; 31:93–117. https://doi.org/10.1002/med.20177 PMID: 19760660

36. Packer L. Antioxidant properties of lipoic acid and its therapeutic effects in prevention of diabetes complications and cataracts. Ann N Y Acad Sci. 1994; 738:257–64. https://doi.org/10.1111/j.1749-6632.1994.tb21811.x PMID: 7832436

37. Berkowitz BA, Bissig D, Roberts R. MRI of rod cell compartment-specific function in disease and treatment in vivo. Prog Retin Eye Res. 2016; 51:90–106. Epub 2015/09/08. https://doi.org/10.1016/j.preteyeres.2015.09.001 PMID: 26344734.

38. Haacke EM, Brown RW, Thompson MR, Venkatesan R. Magnetic Resonance Imaging: Physical Principles and Sequence Design: Wiley; 1999.

39. Berkowitz BA, Lewin AS, Biswal MR, Bredell BX, Davis C, Roberts R. MRI of Retinal Free Radical Production With Laminar Resolution In VivoFree Radical Production With Laminar Resolution In Vivo. Investigative Ophthalmology & Visual Science. 2016; 57(2):577–85. https://doi.org/10.1167/iovs.15-18972 PMID: 26886890

40. Berkowitz BA, Bredell BX, Davis C, Samardzija M, Grimm C, Roberts R. Measuring In Vivo Free Radical Production by the Outer RetinaMeasuring Retinal Oxidative Stress. Investigative Ophthalmology & Visual Science. 2015; 56(13):7931–8.

41. Bissig D, Berkowitz BA. Same-session functional assessment of rat retina and brain with manganese-enhanced MRI. NeuroImage. 2011; 58(3):749–60. https://doi.org/10.1016/j.neuroimage.2011.06.062 PMID: 21749922

42. Cheng H, Nair G, Walker TA, Kim MK, Pardue MT, Thule PM, et al. Structural and functional MRI reveals multiple retinal layers. Proc Natl Acad Sci U S A. 2006; 103(46):17525–30. https://doi.org/10.1073/pnas.0605790103 PMID: 17088544

43. Berkowitz BA, Grady EM, Roberts R. Confirming a prediction of the calcium hypothesis of photoreceptor aging in mice. Neurobiology of Aging. 2014; 35(8):1883–91. https://doi.org/10.1016/j.neurobiolaging.2014.02.020 PMID: 24680323

44. Berkowitz BA, Grady EM, Khetarpal N, Patel A, Roberts R. Oxidative stress and light-evoked responses of the posterior segment in a mouse model of diabetic retinopathy. Invest Ophthalmol Vis Sci. 2015; 56(1):606–15. iovs.14-15687 [pii];10.1167/iovs.14-15687 https://doi.org/10.1167/iovs.14-15687 PMID: 25574049

45. Wang X, Roper MG. Measurement of DCF fluorescence as a measure of reactive oxygen species in murine islets of Langerhans. Anal Methods. 2014; 6(9):3019–24. https://doi.org/10.1039/C4AY00288A PMID: 24955137.

46. Chen X, Zhong Z, Xu Z, Chen L, Wang Y. 2',7'-Dichlorodihydrofluorescein as a fluorescent probe for reactive oxygen species measurement: Forty years of application and controversy. Free Radic Res. 2010; 44(6):587–604. Epub 2010/04/08. https://doi.org/10.3109/10715761003709802 PMID: 20370560.

47. Liu H, Tang J, Du Y, Saadane A, Samuels I, Veenstra A, et al. Transducin1, Phototransduction and the Development of Early Diabetic Retinopathy. Investigative ophthalmology & visual science. 2019; 60(5):1538–46. https://doi.org/10.1167/iovs.18-26433 PMID: 30994864.

48. Pennesi ME, Michaels KV, Magee SS, Maricle A, Davin SP, Garg AK, et al. Long-Term Characterization of Retinal Degeneration in rd1 and rd10 Mice Using Spectral Domain Optical Coherence Tomography. Invest Ophthalmol Vis Sci. 2012; 53(8):4644–56. https://doi.org/10.1167/iovs.12-9611 PMID: 22562504

49. Prusky GT, Alam NM, Beekman S, Douglas RM. Rapid Quantification of Adult and Developing Mouse Spatial Vision Using a Virtual Optomotor System. Investigative Ophthalmology Visual Science. 2004; 45(12):4611–6. https://doi.org/10.1167/iovs.04-0541 PMID: 15557474

50. DOUGLAS RM, ALAM NM, SILVER BD, MCGILL TJ, TSCHETTER WW, PRUSKY GT. Independent visual threshold measurements in the two eyes of freely moving rats and mice using a virtual-reality optokinetic system. Visual Neuroscience. 2005; 22(05):677–84. https://doi.org/10.1017/S0952523805225166 PMID: 16332278

51. Alam NM, Altimus CM, Douglas RM, Hattar S, Prusky GT. Photoreceptor Regulation of Spatial Visual BehaviorPhotoreceptor-Mediated Visual Function. Investigative Ophthalmology & Visual Science. 2015; 56(3):1842–9.

52. Li Y, Zhang Y, Chen S, Vernon G, Wong WT, Qian H. Light-Dependent OCT Structure Changes in Photoreceptor Degenerative rd 10 Mouse Retina. Investigative Ophthalmology & Visual Science. 2018; 59(2):1084–94. https://doi.org/10.1167/iovs.17-23011 PMC5824802. PMID: 29490345

53. Bissig D, Berkowitz BA. Light-dependent changes in outer retinal water diffusion in rats in vivo. Mol Vis. 2012; 18:2561–2xxx. PMID: 23129976

54. Li Y, Fariss RN, Qian JW, Cohen ED, Qian H. Light-Induced Thickening of Photoreceptor Outer Segment Layer Detected by Ultra-High Resolution OCT Imaging. Invest Ophthalmol Vis Sci. 2016; 57(9):Oct105–11. Epub 2016/07/15. https://doi.org/10.1167/iovs.15-18539 PubMed Central PMCID: PMC4968769. PMID: 27409460

55. Cembrowski MS, Spruston N. Heterogeneity within classical cell types is the rule: lessons from hippocampal pyramidal neurons. Nat Rev Neurosci. 2019; 20(4):193–204. Epub 2019/02/20. https://doi.org/10.1038/s41583-019-0125-5 PMID: 30778192.

56. Koutz CA, Wiegand RD, Rapp LM, Anderson RE. Effect of dietary fat on the response of the rat retina to chronic and acute light stress. Exp Eye Res. 1995; 60(3):307–16. https://doi.org/10.1016/s0014-4835(05)80112-5 PMID: 7789410

57. De La PM, Anderson RE. Region and age-dependent variation in susceptibility of the human retina to lipid peroxidation. Invest Ophthalmol Vis Sci. 1992; 33(13):3497–9. PMID: 1464495

58. Mulkey DK, Henderson RA 3rd, Ritucci NA, Putnam RW, Dean JB. Oxidative stress decreases pHi and Na(+)/H(+) exchange and increases excitability of solitary complex neurons from rat brain slices. Am J

Physiol Cell Physiol. 2004; 286(4):C940–51. Epub 2003/12/12. https://doi.org/10.1152/ajpcell.00323.2003 PMID: 14668260.

59. Dmitriev AV, Henderson D, Lau JC, Linsenmeier RA. Retinal Acidosis at an Early Stage of Diabetes in the Rat. ARVO Meeting Abstracts. 2014; 55(5):1049.

60. Majdi A, Mahmoudi J, Sadigh-Eteghad S, Golzari SE, Sabermarouf B, Reyhani-Rad S. Permissive role of cytosolic pH acidification in neurodegeneration: A closer look at its causes and consequences. J Neurosci Res. 2016; 94(10):879–87. Epub 2016/06/11. https://doi.org/10.1002/jnr.23757 PMID: 27282491.

61. Govardovskii VI, Li JD, Dmitriev AV, Steinberg RH. Mathematical model of TMA+ diffusion and prediction of light-dependent subretinal hydration in chick retina. Investigative Ophthalmology & Visual Science. 1994; 35(6):2712–24. PMID: 8188465

62. Berkowitz BA, Podolsky RH, Qian H, Li Y, Jiang K, Nellissery J, et al. Mitochondrial Respiration in Outer Retina Contributes to Light-Evoked Increase in Hydration In Vivo. Invest Ophthalmol Vis Sci. 2018; 59 (15):5957–64. Epub 2018/12/15. https://doi.org/10.1167/iovs.18-25682 PMID: 30551203.

63. Tsai KL, Wang SM, Chen CC, Fong TH, Wu ML. Mechanism of oxidative stress-induced intracellular acidosis in rat cerebellar astrocytes and C6 glioma cells. J Physiol. 1997; 502 (Pt 1):161–74. Epub 1997/07/01. https://doi.org/10.1111/j.1469-7793.1997.161bl.x PMID: 9234204; PubMed Central PMCID: PMC1159579.

64. Okawa H, Sampath AP, Laughlin SB, Fain GL. ATP Consumption by Mammalian Rod Photoreceptors in Darkness and in Light. Current Biology. 2008; 18(24):1917–21. https://doi.org/10.1016/j.cub.2008.10.029 PMID: 19084410

65. Berkowitz BA, Olds HK, Richards C, Joy J, Rosales T, Podolsky RH, et al. Novel imaging biomarkers for mapping the impact of mild mitochondrial uncoupling in the outer retina in vivo. PLOS ONE. 2020; 15 (1):e0226840. https://doi.org/10.1371/journal.pone.0226840 PMID: 31923239

66. Foresta C, Caretta N, Zuccarello D, Poletti A, Biagioli A, Caretti L, et al. Expression of the PDE5 enzyme on human retinal tissue: new aspects of PDE5 inhibitors ocular side effects. Eye (Lond). 2008; 22 (1):144–9. Epub 2007/06/23. https://doi.org/10.1038/sj.eye.6702908 PMID: 17585311.

67. Kang K, Tarchick MJ, Yu X, Beight C, Bu P, Yu M. Carnosic acid slows photoreceptor degeneration in the Pde6b(rd10) mouse model of retinitis pigmentosa. Scientific Reports. 2016; 6:22632. https://doi.org/10.1038/srep22632 PMC4785376. PMID: 26961159

68. Harris A, Kagemann L, Ehrlich R, Ehrlich Y, Lopez CR, Purvin VA. The effect of sildenafil on ocular blood flow. Br J Ophthalmol. 2008; 92(4):469–73. Epub 2008/03/29. https://doi.org/10.1136/bjo.2007.131789 PMID: 18369062.

69. Dias AT, Rodrigues BP, Porto ML, Gava AL, Balarini CM, Freitas FP, et al. Sildenafil ameliorates oxidative stress and DNA damage in the stenotic kidneys in mice with renovascular hypertension. Journal of translational medicine. 2014; 12:35. Epub 2014/02/08. https://doi.org/10.1186/1479-5876-12-35 PMID: 24502628; PubMed Central PMCID: PMC3922021.

70. Semen K, Yelisyeyeva O, Jarocka-Karpowicz I, Kaminskyy D, Solovey L, Skrzydlewska E, et al. Sildenafil reduces signs of oxidative stress in pulmonary arterial hypertension: Evaluation by fatty acid composition, level of hydroxynonenal and heart rate variability. Redox biology. 2016; 7:48–57. Epub 11/22. https://doi.org/10.1016/j.redox.2015.11.009 PMID: 26654977.

71. Walker DK, Ackland MJ, James GC, Muirhead GJ, Rance DJ, Wastall P, et al. Pharmacokinetics and metabolism of sildenafil in mouse, rat, rabbit, dog and man. Xenobiotica. 1999; 29(3):297–310. Epub 1999/04/29. https://doi.org/10.1080/004982599238687 PMID: 10219969.

72. Nakano M, Lockhart CM, Kelly EJ, Rettie AE. Ocular cytochrome P450s and transporters: roles in disease and endobiotic and xenobiotic disposition. Drug metabolism reviews. 2014; 46(3):247–60. https://doi.org/10.3109/03602532.2014.921190 PMC4676416. PMID: 24856391

73. Chang Q, Berdyshev E, Cao D, Bogaard JD, White JJ, Chen S, et al. Cytochrome P450 2C epoxygenases mediate photochemical stress-induced death of photoreceptors. J Biol Chem. 2014; 289 (12):8337–52. Epub 2014/02/13. https://doi.org/10.1074/jbc.M113.507152 PMID: 24519941; PubMed Central PMCID: PMC3961660.

74. Sandner P, Hütter J, Tinel H, Ziegelbauer K, Bischoff E. PDE5 inhibitors beyond erectile dysfunction. International journal of impotence research. 2007; 19(6):533–43. https://doi.org/10.1038/sj.ijir.3901577 PMID: 17625575

75. Carter-Dawson LD, Lavail MM, Sidman RL. Differential effect of the rd mutation on rods and cones in the mouse retina. Investigative Ophthalmology Visual Science. 1978; 17(6):489–98. PMID: 659071

76. Wang T, Reingruber J, Woodruff ML, Majumder A, Camarena A, Artemyev NO, et al. The PDE6 mutation in the rd10 retinal degeneration mouse model causes protein mislocalization and instability and promotes cell death through increased ion influx. J Biol Chem. 2018; 293(40):15332–46. Epub 2018/08/22. https://doi.org/10.1074/jbc.RA118.004459 PMID: 30126843; PubMed Central PMCID: PMC6177582.

77. Power M, Das S, Schutze K, Marigo V, Ekstrom P, Paquet-Durand F. Cellular mechanisms of hereditary photoreceptor degeneration—Focus on cGMP. Prog Retin Eye Res. 2019:100772. Epub 2019/08/03. https://doi.org/10.1016/j.preteyeres.2019.07.005 PMID: 31374251.